

# Rapid Deposition of the Biomimetic Hydroxyapatite-Polydopamine-Amino Acid Composite Layers onto the Natural Enamel

Pavel Seregin,\* Dmitry Goloshchapov, Anna Emelyanova, Konstantin Eremeev, Yaroslav Peshkov, Khidmet Shikhaliev, Andrey Potapov, Yury Ippolitov, Vladimir Kashkarov, Dmitry Nesterov, Kirill Shapiro, Raul O. Freitas, and Iman. A. Mahdy



Cite This: *ACS Omega* 2024, 9, 17012–17027



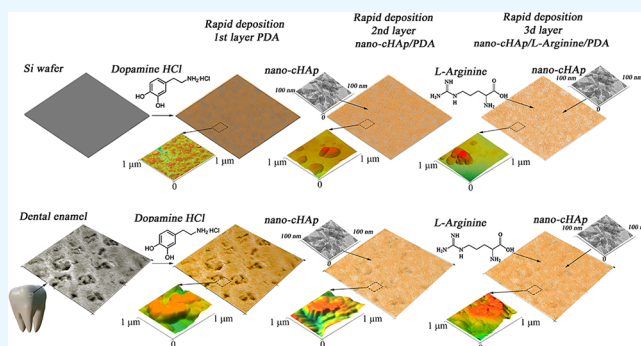
Read Online

ACCESS |

Metrics & More

Article Recommendations

**ABSTRACT:** In this work, we developed a technology that enables rapid deposition of biomimetic composite films onto natural enamel slices (known as biotemplates). These films are composed of polydopamine (PDA) and nanocrystalline carbonate-substituted hydroxyapatite (nano-cHAp) that have been functionalized with amino acid L-Arginine. We utilized atomic force microscopy (AFM) and scattering scanning near-field optical microscopy (s-SNOM) combined with infrared (IR) synchrotron to achieve nanoscale spatial resolution for both IR absorption and topography analyses. This combined analytical modality allowed us to understand how morphology connects to local changes in the chemical environment on the biotemplate surface during the deposition of the bioinspired coating. Our findings revealed that when using the proposed technology and after the deposition of the first PDA layer, the film formed on the enamel surface nearly covers the entire surface of the specimen whose thickness is larger on the surface of the emerging enamel prisms. Calculation of the crystallinity index for the biomimetic layer showed a multiple increase compared with natural enamel. This indicates regular and dense aggregation of nano-cHAp into larger crystals, imitating the morphology of natural enamel rods. The microhardness of the formed PDA-based biomimetic layer mineralized with nano-cHAp functionalized with amino acid L-Arginine deposited on natural enamel was practically the same as that of natural enamel. The characterization of nano-cHAp-amino acid-PDA layers using IR and Raman microspectroscopy showed that L-arginine acts as a conjunction agent in the formation of mineralized biomimetic composite coatings. The uniformity of the mechanisms of PDA layer formation under different deposition conditions and substrate types allows for the formation of coatings regardless of the macro- and micromorphology of the template. Therefore, the results obtained in this work have a high potential for future clinical applications in dental practice.



## 1. INTRODUCTION

Dental composites containing bioinspired mineral and organic components such as nanocrystalline hydroxyapatite, amino acids, polymers, etc. are the subject of current topical research.<sup>1–3</sup> These smart materials are in demand to restore lost dental hard tissue as part of the biomimetic approach in dentistry, where it becomes possible to restore the function and vitality of teeth through restorations.<sup>2–5</sup> This requires imitating the natural tissue: the fibrous structure and morphology of the dental organomineral complex with its unique biomechanical properties.<sup>3,5,6</sup>

Since hydroxyapatite nanocrystals (HAp) are the initial inorganic substances in solid tissues,<sup>7</sup> it is biomimetic layer-by-layer mineralization that is considered to be the ideal strategy to build an apatite-like layer (interface) on the surface of the restorative mineralized tissue.<sup>8</sup> However, in order to implement the biomineralization process, it is necessary to use an

organic matrix that controls the assembly of inorganic crystals to form organomineral hybrid apatite-like materials.<sup>9,10</sup> In this process of biomimetic mineralization, it becomes possible to control the morphology, composition, and growth of crystals in different dimensions, which are regulated by biomolecules, proteins, and amino acids.<sup>9–11</sup>

Earlier in several works, it was shown that it is possible to control the morphology, hierarchy, and size of structural units of dental tissue (hydroxyapatite nanocrystals) using protein matrix subunits—polar amino acids.<sup>9,10,12,13</sup> In vitro studies

**Received:** October 27, 2023

**Revised:** March 19, 2024

**Accepted:** March 26, 2024

**Published:** April 8, 2024



have shown that, like proteins, charged amino acids can either inhibit or induce hydroxyapatite mineralization.<sup>10,11,14</sup> One of such important amino acids for the human body is L-Arginine, which can be used as a growth modifier of hydroxyapatite particles.<sup>15,16</sup> Thus, in the presence of L-Arginine below the isoelectric point, HAp nanocrystals with lamellar morphology are formed, and above the isoelectric point, those with rod-shaped morphology are formed.<sup>16</sup> However, the effectiveness of L-Arginine to induce the growth of hydroxyapatite particles may depend on the pH of the solution, resulting in a change in the conformational environment for bond formation with nanocrystalline carbonate-substituted hydroxyapatite (nano-cHAp).<sup>17</sup> In this case, the change in the physicochemical properties of the formed biocomposite can occur through several mechanisms, one of which is the substitution of calcium (Ca<sup>+</sup>) and hydroxides (OH<sup>-</sup>) in the crystal structure of nano-cHAp by amino acid functional groups.<sup>10,12,14</sup> Moreover, the operation of different amino acid matrices allows for control of not only the process of hydroxyapatite deposition and the formation of an apatite-like layer, but also the molecular and charge properties of the surface of the deposited coating, which in turn can contribute to the adsorption of proteins on it.<sup>18</sup>

At the same time, the introduction of organic polymers into the composition of bioinspired material allows us to achieve chemical modification and functionalization of the formed biomimetic layer, as well as to bind it to the natural mineralized tissue.<sup>3,19–21</sup> Recently, a nature-like adhesive, polydopamine (PDA),<sup>1</sup> which contains a variety of functional molecular groups, including amine, catechol, and quinone groups,<sup>22</sup> has shown high potential for clinical application.<sup>1,21,23</sup> Due to this, PDA is able to form strong bonds with the surface of almost all known materials regardless of their chemical composition. In particular, it is known that PDA is able to bind to Ca<sup>2+</sup> ions of hydroxyapatite through functional groups, which contributes to the formation of a biomimetic mineralized layer.<sup>2,24</sup> Recently, it has been suggested that codeposition of phosphates with polydopamine (PDA) may be a simple and promising strategy to activate enamel and dentin mineralization and modify their surface.<sup>25</sup> The hybrid organomineral interfaces thus formed may facilitate the regeneration of enamel-like layers in dental defect repair procedures. To date, Yan et al. have successfully constructed a biomimetic organo-inorganic integrated interface on dentin by forming hybrids of calcium phosphate and collagen using cross-linking.<sup>26</sup> Although already developed biomimetic techniques can be used to restore a dental hard tissue structure using biomimetic organo-inorganic interfaces,<sup>19</sup> they often take at least a week. Thus, an important challenge is to realize the rapid and efficient development of a biomimetic organo-inorganic interface for dental hard tissue restoration.

It should be noted that this rather simple approach for the formation of multilayer biomimetic coatings based on nano-cHAp, amino acids, and PDA by layer-by-layer accelerated deposition should obviously not affect the intrinsic properties of the biocomposite.<sup>21,27,28</sup> However, the process of material formation from multiple components is still quite complex.<sup>2,3,29</sup> The properties of the biocomposite will depend on both the ratio of components and the kind of interaction between them and the synthesis conditions (temperature, pH, concentration, reaction time, etc.). Moreover, in multilayer deposition, the fact that the biomimetic layer inherits the properties (morphological organization) of the substrate on which the coating formation technique has been developed is

undoubtedly a problem.<sup>19,30,31</sup> This is not always acceptable when translating or adapting the technology for other objects. Also open is the methodological problem of obtaining homogeneous or homogeneous coatings on a wide scale in “dirty” conditions characteristic of clinical practice.

The described problem of forming a biomimetic nano-cHAp-amino acid-PDA composite is an interdisciplinary problem for tissue engineering, and the currently available data on its solution in the literature are illustrative rather than exhaustive and require additional research.

Therefore, the aim of our work was to investigate the effect of L-Arginine on rapid deposition of the biomimetic hydroxyapatite-polydopamine-amino acid composite layers onto natural enamel.

## 2. MATERIALS AND METHODS

**2.1. Materials.** **2.1.1. Research Design.** Rapid deposition of polydopamine-based films followed by mineralization procedures of the coatings using nonstoichiometric nano-cHAp, including polar amino acid functionalization, was carried out in several steps with different deposition times.

Polished plates of monocrystalline silicon with (111) orientation were used as substrates to develop the technology of biomimetic layer formation, as described in ref 32. The use of silicon wafers is due to practical convenience for identification and diagnostics of molecular composition, surface morphology, and thickness of deposited nano-composite biomimetic films. Since the screening of the formed layers is performed using molecular analysis and probe microscopy methods, in the case of silicon wafers, it is much easier to separate the signal from the film and foreign substrate, as well as to control the surface morphology features of the layers.

To assess the applicability of the developed approaches to dental practice, at the next stage, the deposition of layers was performed on the surface of natural enamel of human teeth (biotemplates). Samples of natural enamel (slices) were obtained similarly<sup>33</sup> from healthy teeth extracted for orthodontic indications (without carious lesions and erosions). The teeth were extracted from donors aged 20–25 years and collected in accordance with relevant guidelines and regulations. After extraction, the specimens were immediately cleaned and placed in separate vials containing 0.9% physiological saline and 0.002% sodium azide and stored at 4 °C. Dental enamel slices were obtained using a water-cooled diamond low-turn saw. After the segmentation procedure, the tooth enamel slices were placed in airtight containers with constant humidity, where they were stored until the experiments were performed.

Approaches to the preparation of starting reagents and conditions for film deposition as well as pretreatment of substrates and biotemplates are summarized below.

**2.1.2. Substrate Surface Pretreatment Procedure.** Silicon wafers and biotemplates were pretreated in the same way. As an initial treatment for surface profiling, the wafers were incubated for 30 s in 38% orthophosphoric acid (H<sub>3</sub>PO<sub>4</sub>) solution and then washed for 60 s in distilled water. The substrates were then incubated for 30 s in 12% calcium hydroxide (Ca(OH)<sub>2</sub>) solution. As shown in previous studies,<sup>33,34</sup> this procedure leads to the formation of a stable amino acid-hydroxyapatite bond and benefits the formation of textured coatings. After treatment, the samples were placed in a

vessel with distilled water until the beginning of the experiment (1 h).

**2.1.3. Obtaining Nano-cHAp for the Mineralization Procedure.** To obtain nanocrystalline carbonate-substituted hydroxyapatite with structural and morphological organization of crystals similar to apatite of natural enamel, the technique of liquid-phase precipitation from solution was used.<sup>35</sup> Calcium carbonate obtained from bird eggshells and a 0.3 M solution of orthophosphoric acid ( $\text{H}_3\text{PO}_4$ ) were used as initial reagents. The use of  $\text{Ca}(\text{CO}_3)$  synthesized from a biogenic source of calcium is justified by the possibility of synthesizing powders of nanocrystalline carbonate-substituted hydroxyapatite, which is similar to natural enamel apatite in terms of trace element composition, structure, and morphology.<sup>35–37</sup> In the nano-cHAp preparation step, calcium carbonate was annealed at 950 °C. After cooling to 50 °C,  $\text{Ca}(\text{CO}_3)$  was mixed with distilled water to obtain a paste-like consistency and form  $\text{Ca}(\text{OH})_2$ . A part of the obtained calcium hydroxide was used to treat the substrates (templates), and the other part was titrated with 0.3 M orthophosphoric acid solution to synthesize nano-cHAp. The titration was performed for 1.5 h at  $T = 28$  °C until pH 8 was reached (monitored using pH meter/ionmeter/titrator IPL 111–1). Throughout the titration process, the solution was stirred using a magnetic stirrer (800 rpm). After the suspension was obtained and allowed to stand for 24 h, the precipitate was filtered, dried, and dispersed. The obtained nanocrystalline hydroxyapatite was added to TRIS (pH = 8.7) to obtain a suspension concentration of 0.25 mg/mL immediately prior to the template mineralization procedure. The chosen concentration was selected to prevent accelerated agglomeration of nano-cHAp in solution.<sup>38</sup> The resulting final suspension was treated five times in ultrasound [using Qsonica ultrasonic homogenizer (LLC, CT, USA), 55W transmitter power, 100% amplitude] for 1 min with pauses of 5 min each to prevent the solution from overheating.

**2.1.4. Functionalization of Nano-cHAp by the Amino acid L-Arginine.** For functionalization of nano-cHAp, solutions with increased L-Arginine content (1.5 mg/mL) were used. For this purpose, L-Arginine at a concentration of 1.5 mg/mL was injected into the previously obtained TRIS solution (pH = 8.7) containing nano-cHAp (0.25 mg/mL) immediately after ultrasonic treatment of the suspension. An orbital shaker at 120 rpm was used to homogenize the solution. The mixing dwell time was 30 min before the start of the substrate treatment.

**2.1.5. Preparation of Dopamine Hydrochloride.** For our studies, dopamine hydrochloride was prepared using 1.81 g of 2-(3,4-dimethoxyphenyl) ethan-1-amine and 10 mL of concentrated hydrochloric acid.<sup>24</sup> The reagents were annealed in a sealed ampule at 150 °C for 2 h. The obtained product was subjected to drying to form a dry residue. The purification procedure of the obtained residue was carried out by column chromatography on silica gel (60  $\mu\text{m}$ ), and the eluent was methanol. Methanol elution was subsequently carried out. The residue obtained was recrystallized from 20% hydrochloric acid to give a dopamine hydrochloride powder. The product obtained after columnar chromatography was subjected to recrystallization, which proves to be an additional purifying. The formation of hydrochloride was recorded using Bruker DRX500 NMR spectroscopy (500 MHz) in  $\text{DMSO}-d_6$ , internal standard TMS, and high-resolution mass spectroscopy [Agilent Technologies LCMS TOF 6230B, ionization

method—double electrospray in nitrogen atmosphere (dual-ESI)].

**2.1.6. Polymerization and Deposition of PDA Films.** For dopamine polymerization, we used a technique that allows us to obtain both thin and thick PDA layers in a short period of time.<sup>32</sup> The advantages of the technique include the uniformity and homogeneity of the deposited coatings, as well as a high deposition rate of  $\sim 43$  nm/h.<sup>32</sup> TRIS buffers (pH = 8.7.) with a dopamine hydrochloride concentration of 2 mg/mL were used to obtain polydopamine film. For accelerated deposition of polydopamine film, 5 mM of  $\text{CuSO}_4 \cdot 6\text{H}_2\text{O}$  solution and 20 mM  $\text{H}_2\text{O}_2$  were added to the initiating solution at a constant stirring speed of 200 rpm, and 20 mM  $\text{H}_2\text{O}_2$  was added at the time. The introduction of  $\text{CuSO}_4 \cdot 6\text{H}_2\text{O}$  provides the formation of reactive ionic complexes that promote the accelerated oxidation of polydopamine.<sup>32,39</sup>

**2.1.7. Description of the Samples Studied.** The alternation of PDA and nano-cHAp layers in the formation of the mineralized layer has been used to reproduce the hierarchical structure of tooth enamel, in which nanocrystals of substituted calcium apatite alternate with nanolayers of the organic matrix interfacing them.<sup>3,19,40</sup> The alternation of layers should contribute to uniform filling of the template surface, achieve stable conjugation of hydroxyapatite crystals, and increase the thickness of coatings with a reproducible film structure, which in turn is important for practical applications.<sup>3,19,31,41</sup>

The samples studied in this article have the following design.

**2.1.7.1. Sample S1.** A reference plate of single-crystalline silicon Si (111) was used.

**2.1.7.2. Sample S2.** A Si (111) monocrystalline silicon wafer was used as a substrate. Initially, pretreatment of the substrate was performed. The PDA film was then deposited 3 times, with a fresh solution used at each step. Considering that the deposition rate is slightly higher at the initial time point<sup>32</sup> and it has a nonlinear nature, and taking into account the fact that the initially formed PDA layers have a large number of heterogeneous bonds, the estimated calculated thickness of the coating is  $\sim 90$  nm.<sup>32,39</sup>

**2.1.7.3. Sample S3.** A Si (111) monocrystalline silicon wafer was used as a substrate. Initially, pretreatment of the substrate was carried out, and after that, the initial deposition of the PDA film was performed. Next, the substrate was placed in TRIS buffer (pH = 8.7) containing synthesized nano-cHAp (0.25 mg/mL) pretreated by ultrasound. After the mineralization procedure using nano-cHAp was performed for 30 min, a second layer of PDA was obtained. Next, the mineralization procedure was repeated by using nano-cHAp for 30 min. After that, a third layer of PDA was deposited. Each time, a new solution of dopamine hydrochloride was used to deposit the PDA film. The estimated thickness of the film obtained during multiple depositions is  $\sim 150$  to 200 nm.

**2.1.7.4. Sample S4.** A Si (111) monocrystalline silicon wafer was used as a substrate. Initially, substrate pretreatment was performed. After that, PDA film deposition was performed 2 times, with fresh solution used at each step. Next, the substrate was placed in TRIS solution (pH = 8.7.) containing nano-cHAp functionalized with the amino acid L-Arginine. After 30 min of exposure to this solution, the third layer of PDA was deposited.

**2.1.7.5. Sample S5.** Reference (slice): natural enamel.

**2.1.7.6. Sample S6.** A slice of natural enamel (biotemplate) was used as a substrate. Initially, the substrate was pretreated.

Table 1. Sequence of Technological Procedures for Obtaining Samples

sample No	H <sub>3</sub> PO <sub>4</sub> 30 s Ca(OH) <sub>2</sub> 30 s	PDA— 2 mg/mL 30 min	Nano-cHAP 0.25 mg/mL 30 min	PDA— 2 mg/mL 30 min	Nano-cHAP 0.25 mg/mL 30 min	L-arginine 1.5 mg/mL	PDA s— 2 mg/mL 30 min
S1							
S2	+	+		+			+
S3	+	+	+	+	+		+
S4	+	+		+	+	+	+
S5							
S6	+	+		+			+
S7	+	+	+	+	+		+
S8	+	+		+	+	+	+

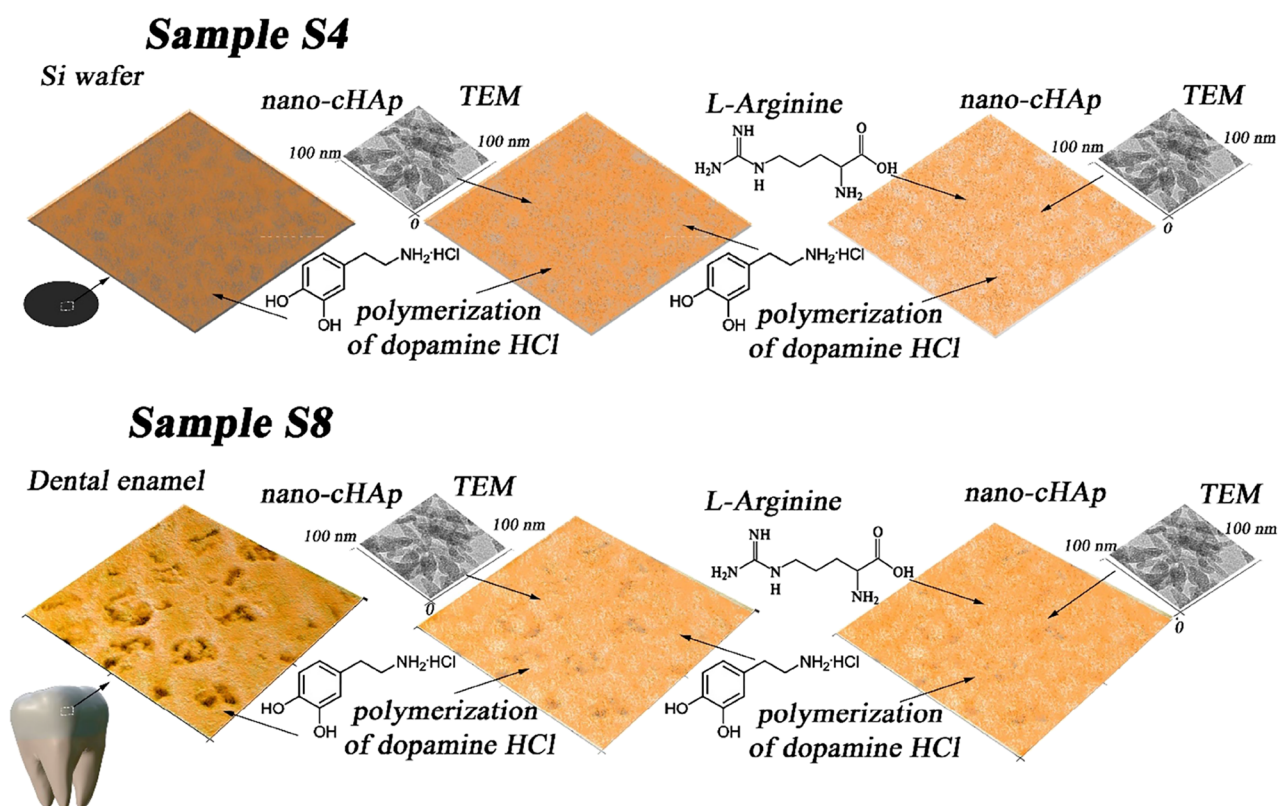


**Figure 1.** Process design for deposition of a polydopamine-based mineralized biomimetic layer on the silicon substrate (sample S4) and biotemplate (sample S8).

Then the PDA film was deposited 3 times, with fresh solution used at each step. The estimated coating thickness is  $\sim 90$  nm.

**2.1.7.7. Sample S7.** A slice of natural enamel (biotemplate) was used as a substrate. Initially, the substrate was pretreated, and then the initial deposition of the PDA film was performed. Next, the substrate was placed in TRIS solution ( $\text{pH} = 8.7$ ) containing nano-cHAp (0.25 mg/mL) pretreated with ultrasound. After performing the mineralization procedure using nano-cHAp for 30 min, a second layer of PDA was obtained. Next, the mineralization procedure was repeated using nano-cHAp for 30 min. After that, a third layer of PDA was deposited. Each time, a fresh solution of dopamine hydrochloride was used to deposit the PDA film. The estimated thickness of the film obtained during multiple deposition is  $\sim 150$  to 200 nm.

**2.1.7.8. Sample S8.** A slice of natural enamel (biotemplate) was used as a substrate. Initially, the substrate was pretreated. After that, deposition of the PDA film was performed 2 times, with fresh solution used at each step. Next, the substrate was placed in TRIS solution ( $\text{pH} = 8.7$ ) containing nano-cHAp

functionalized with the amino acid L-Arginine. After 30 min exposure to this solution, the third layer of PDA was deposited.

The list of samples and completed process steps is presented in Table 1.

Figure 1 shows a schematic representation of the biomimetic layer deposition processes for samples S4 and S8.

It should be noted that during the formation of PDA-based biomimetic layers (see Figure 1), a PDA layer was first deposited on the pretemplate surface (Si wafer or natural enamel), which is important for obtaining further homogeneous coatings. The calculated thickness of the first layer according to ref 32 should be at least 20 nm. The formation of samples with different conditions and layer thicknesses is necessary to identify the most suitable conditions for the deposition of the second PDA layer on the surface of the first layer (Figure 1). In this case, to establish the influence of the amino acid L-Arginine on the formed morphology of HAp-PDA layers, the third PDA layer (samples S4 and S8, Figure 1), mineralized with nano-cHAp functionalized with the amino

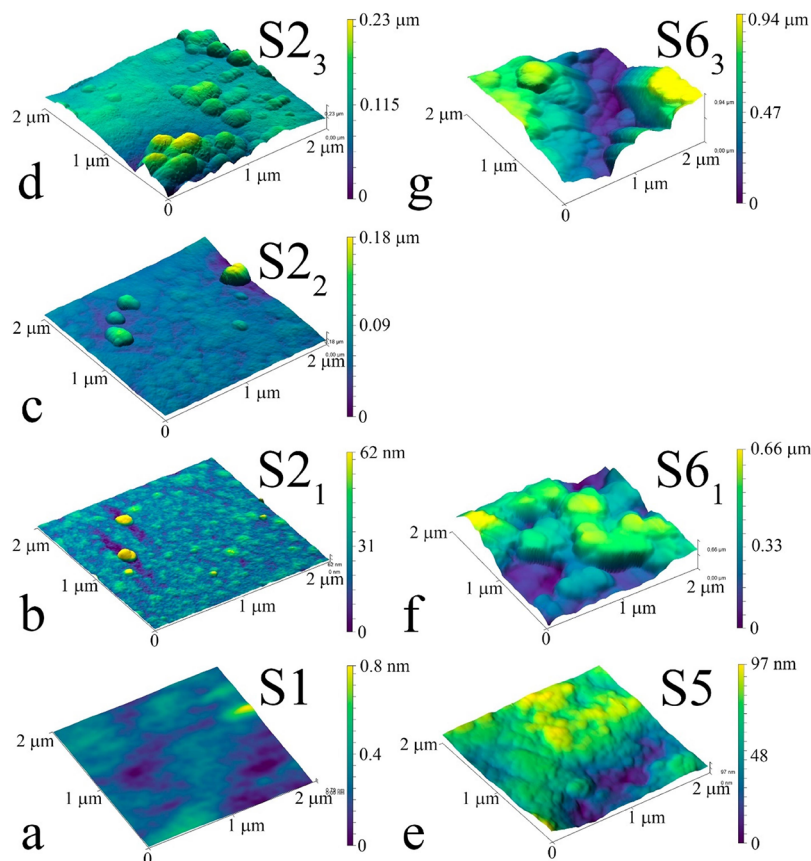


**Figure 2.** AFM images of surface areas of  $2 \times 2 \mu\text{m}^2$  samples: (a) polished crystalline silicon plate (sample S1); (b–d) after applying one (sample S2<sub>1</sub>), two (sample S2<sub>2</sub>), and three (sample S2<sub>3</sub>) layers of PDA to the pretreated crystalline silicon plate, respectively; (e) human tooth enamel (sample S5); (f, g) after applying one (sample S6<sub>1</sub>) and three (sample S6<sub>3</sub>) layers of PDA to the pretreated enamel surface, respectively.

acid L-Arginine, was deposited, and the results were compared with samples S3 and S7.

**2.1.8. Characterization Methods. 2.1.8.1. Optical Microscopy.** Optical images of surface areas of samples N1–N5 were obtained by using an Olympus CX40 optical microscope. An Olympus 40 $\times$ /0.65 planachromatic lens and a Levenhuk 5 MPix digital camera were used for imaging. The images were obtained from the central area of each sample in light field mode with a flat field correction. The size of the studied area on the surface of the samples was  $300 \times 400 \mu\text{m}$  at  $\times 400$  magnification. The images were analyzed using the TaupTek TaupView software package (Hangzhou Touptek Photonics Co., China).

**2.1.8.2. Atomic Force Microscopy.** The surface morphology was studied using a Femtoscan-001 NT MDT scanning probe microscope in atomic force microscopy mode. The surface morphology was studied using a Femtoscan-001 NT MDT scanning probe microscope in atomic force microscopy mode.

**2.1.8.3. IR Nanoimaging.** IR s-SNOM experiments were performed at the Brazilian Synchrotron Light Laboratory (LNLS) in the IMBUA-nano endstation. Single frequency near-field imaging was performed using a set of Quantum Cascade Laser (QCL) sources (MirCat, DRS Daylight Solutions Inc.) covering from 930 to 1730  $\text{cm}^{-1}$  with a minimum frequency step of 1  $\text{cm}^{-1}$ . Power at the sample was set to be no higher than 1 mW. To acquire both amplitude and phase of the scattered signal, the optical setup was set as a pseudo-Heterodyne (psHet) scheme in a commercial asymmetric Michelson interferometer (neaSNOM, Neaspec

GmbH), where the reference mirror was mounted in a fast-scanning stage for background suppression and phase decoupling.<sup>42,43</sup> For mid-IR optical processing, we used a ZnSe beamsplitter and a mercury cadmium telluride detector (MCT, Kolmar Technologies Inc.) for the interferometric setup. Platinum–iridium (PtIr) AFM tips (Nanosensors PPP-NCHPt, NanoWorld AG) were used as probes. The s-SNOM microscope is an atomic force microscope that operates in semicontact (tapping) mode with a fundamental mechanical frequency  $\Omega$  of  $\sim 250$  kHz. A custom-designed optics collects and focuses the incident tunable narrowband beam at the AFM tip, inducing an effective polarization of the tip that enhances light interaction with the sample. The optical near-field signal ( $S_m$ ), which emerges from a sample region comparable to the tip radius ( $\sim 25$  nm), is extracted from the detected backscattered light by demodulating the signal at higher harmonics ( $m$ ) of  $\Omega$ , via lock-in amplifier detection.

**2.1.8.4. Infrared Spectroscopy.** IR spectra of the obtained composite films on silicon wafer were observed in the range of 4500–400  $\text{cm}^{-1}$  with a Vertex-70 (Bruker) spectrometer employing the attenuated total reflectance attachment (ATR) PlatinumATR. Transmittance spectra were registered with a step of 2  $\text{cm}^{-1}$ . Processing of the spectral data, normalization, and background correction were performed with the use of the Origin 9.0 program suite.

**2.1.8.5. Raman Microspectroscopy.** Molecular properties of the formed biomimetic layers were studied on the basis of point Raman spectral analysis, which is an effective approach for the analysis of materials with biological nature. Spectra

were obtained using a confocal Raman microscope RamMix 532 (InSpectr, Moscow, Russia) with 532 and 785 nm wavelength laser excitation and 10 mW of radiation power at the sample. Spectra were collected in the range of 200–2000  $\text{cm}^{-1}$  with a spectral resolution of 1  $\text{cm}^{-1}$ . The selection of the region of interest in the sample surface was performed using an automated motorized two-axis stage, allowing the sample to be moved in the scanning plane with a step of 250 nm. The signal from the sample surface was collected using a 100 $\times$  objective lens, and the area of the analyzed region was  $1 \times 1 \mu^2$ .

Processing of the collected Raman spectral data included baseline correction, normalization, and noise reduction with Savitzky-Golay smoothing and was performed using Origin software. The spectra were normalized by using vector normalization. Savitzky-Golay smoothing parameters were the fourth degree of polynomial, second-order derivative, and 67 smoothing points. For optimization, the baseline-corrected raw data in the spectral range of wave numbers 2000–200  $\text{cm}^{-1}$  were compared with the baseline-corrected spectra.

**2.1.8.6. Low-Angle XRD.** X-ray diffraction from shallow depths was studied by using low angle X-ray diffraction. We used an ARL X'TRA X-ray diffractometer and  $\text{CuK}\alpha$  radiation ( $\lambda = 1.5406 \text{ \AA}$ ). The instrument was operated in step-scan mode with a step of  $2\theta = 0.02^\circ$  and an accumulation of 5 s/point. The tilt angle  $\alpha$  was experimentally selected to ensure the optimal depth of the diffracted radiation output, taking into account the thickness of the deposited biomimetic layer.

**2.1.9. Microhardness Measurement.** Surface microhardness was measured using Vicker's diamond machine. Indentations were done for the specimens by a pyramid diamond indenter tip with a 50 g load for 10 s. The indentations were measured using built in a microscope, and Vickers hardness (HV) was calculated using  $\text{HV} = 1854.4 L/d^2$  where the load  $L$  is in kgf and  $d$  is the diameter of the prism in  $\mu\text{m}$ . The mean of the five indentations' results was used to calculate the average hardness value for each sample.

### 3. FINDINGS AND DISCUSSION

It has been repeatedly demonstrated<sup>44,45</sup> that during deposition of PDA-based biomimetic layers, including for the purpose of mineralization of dental tissue, the key factor determining both the deposition rate and the quality of coatings is the mechanism of dopamine polymerization. In this case, the deposition technology of PDA layers can be successfully controlled using standardized substrates with known roughness and composition.<sup>32</sup> Therefore, the technology and conditions for rapid deposition of PDA nanofilms with controlled thickness and uniformity were initially worked out. For this purpose, polished and pretreated Si(111) silicon wafers were used as substrates to control the growth of the films. Preliminary visual analysis of the deposited layers using optical microscopy revealed the formation of a continuous coating of silicon wafers with a PDA-based film.

The morphology of the formed biomimetic layers was studied in more detail by using probe microscopy (AFM). Figure 2 shows AFM images of the surface of samples for which PDA-based films were deposited on both Si wafers (Figure 2a–d) and biotemplates (Figure 2e–g).

AFM images of sample S2 show its surface morphology after deposition was performed: one layer (S21), two successive layers (S22), and three successive layers (S23) (Figure 2b–d). For comparison, Figure 2 also shows the AFM surface

topology of a reference polished crystalline silicon wafer (sample S1, Figure 2a).

AFM studies confirmed that after pretreatment of silicon wafers using orthophosphoric acid and calcium hydroxide, surface profiling with increasing roughness occurred, which favored the deposition of PDA films. Further accelerated deposition of PDA layers resulted in the formation of coatings of different thicknesses. It is clearly seen that after the first step of PDA deposition on the surface of the Si(111) wafer, the formation of a film is observed, the thickness of which does not exceed 35 nm according to the results of AFM profiling (Figure 2b, sample S2<sub>1</sub>). Despite the rather high rate of coating formation, the formation of individual large agglomerates on the surface is simultaneously observed with sizes ranging from 100 to 150 nm (Figure 2b). AFM images demonstrate that after deposition of the second PDA layer (Figure 2c, sample S2<sub>2</sub>), the coating morphology is different from that observed after a single deposition (Figure 2b, sample S2<sub>1</sub>). A more homogeneous distribution of the formed film is noticeable on the surface, and the thickness of the film itself reaches  $\sim 80$  nm. The agglomerates observed on the surface are spherical in shape reaching  $\sim 250 \times 250 \times 150$  nm (Figure 2c, sample S2<sub>2</sub>). The deposition of a third layer of PDA leads to an even more uniform distribution of agglomerates and nanoparticles on the sample surface (Figure 2d, sample S2<sub>3</sub>). The maximum height of the ASM profile in this case is 700 nm. It can be observed that some of the deposited PDA particles are attached to the previously formed aggregates, which is quite logical due to the appearance of more bonds between PDA particles than with the substrate. Individual characteristic agglomerates have dimensions of  $500 \times 500 \times 100$  nm (Figure 2d, sample S2<sub>3</sub>). Importantly, the formation of the characteristic layered structure of the PDA layer is clearly visible in AFM images beneath the large agglomerates/particles.<sup>46,47</sup> PDA-based coatings always contain a layered structure formed by quasi-planar clusters underneath, as well as large PDA aggregates on the surface, which is in agreement with previously published data.<sup>22,47,48</sup> As mentioned earlier, the formation of layered structures during coating deposition is related to the supramolecular structure of PDA molecules and their ordered deposition on substrates.<sup>46</sup> The results confirm that the thickness of the PDA layer increases with deposition time, while multiple film deposition using fresh solutions helps to achieve uniformity in the distribution of the formed film while reducing the deposition time and is a reliable approach to creating PDA coatings.

The proven technology was adapted for the deposition of PDA layers on biotemplates. For this purpose, natural enamel slices pretreated with orthophosphoric acid and calcium hydroxide were used, on which three PDA layers were deposited. An AFM image of the surface of such a coating is shown in Figure 2f (sample S6<sub>3</sub>), and for comparison, images of the surface of the same sample after the deposition of one layer of PDA (sample S6<sub>1</sub>) and the natural enamel reference (sample S5) are shown. It can be clearly seen (Figure 2e–g) that the intrinsic morphology of the pretreated biotemplate has a significant effect on the PDA layers deposited on it and, in particular, on the size of the PDA aggregates on the surface of the quasi-planar film covering the enamel. Comparison of the topology of samples S6<sub>1</sub> (PDA layer deposited on natural enamel) and S2<sub>1</sub> (PDA layer deposited on a silicon wafer), for which identical pretreatment and deposition procedures were performed, indicates that the biotemplate film is thicker

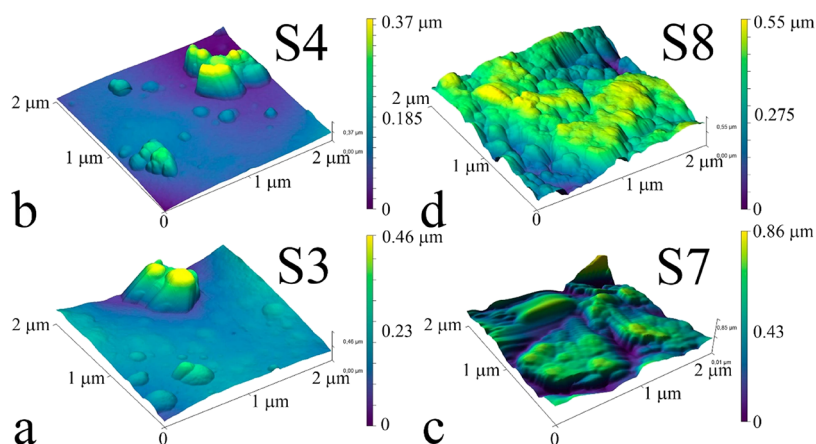


**Figure 3.** AFM images of surface areas of  $2 \times 2 \mu^2$  samples: (a) PDA-based biomimetic layer mineralized using nano-cHAP deposited on a silicon wafer (sample S3); (b) PDA-based biomimetic layer mineralized using nano-cHAP functionalized with the amino acid L-Arginine, deposited on a silicon wafer (sample S4); (c) PDA-based biomimetic layer mineralized with nano-cHAP deposited on natural enamel (sample S7); (d) PDA-based biomimetic layer mineralized with nano-cHAP functionalized with the amino acid L-Arginine deposited on natural enamel (sample S8).

(Figure 2b,f). It was previously demonstrated that when the silicon surface was functionalized with glycoproteins, there was an increase in the thickness of the deposited PDA film.<sup>48</sup> Therefore, in view of the different chemical compositions of the substrates used as well as the presence of a large number of chemical bonds in enamel, an increase in the thickness of the deposited PDA film is a natural consequence of the nature of the biotemplate. At the same time, as the number of deposited layers on the enamel surface increases (see Figure 2f,g, samples S6<sub>1</sub> and S6<sub>3</sub>), the size of PDA agglomerates increases up to submicron units.

The morphology of the biomimetic layer based on PDA mineralized using nano-cHAP as well as nano-cHAP functionalized with the amino acid L-Arginine, when the coatings were deposited on silicon wafer (samples S3 and S4, respectively) as well as natural enamel slices (samples S7 and S8, respectively), is shown in Figure 3.

In the case of mineralization of PDA film using nano-cHAP (sample S3, Figure 3a), the lower sublayer is formed by a nonhomogeneous distribution of large quasi-planar agglomerates, and in the upper sublayer, the formation of inhomogeneities up to half-micrometer size is observed. At the same time, on the whole surface of sample S4 (see Figure 3b), for which nano-cHAP was functionalized using L-Arginine, a much more homogeneous distribution of particles with sizes on the order of 70 nm is recorded, which is comparable to the parameters of the nano-cHAP used. A similar pattern is observed in the case of deposition of typical PDA layers on the biotemplate surface (natural enamel slices). It is seen that the surface of sample S7 (Figure 3c) shows features characteristic of the morphology of enamel coated with a PDA mineralized layer containing nano-cHAP. It is possible to notice rather laterally large agglomerates of the mineralized layer deposited preferentially in the places where the enamel apatite prisms come to the surface. The use of nano-cHAP functionalized with L-Arginine in the deposition of the biomimetic PDA layer on natural enamel slices (sample S8, Figure 3d) promotes a homogeneous distribution of surface-forming nanocrystals. It is likely that in this case, the binding of the PDA film to the organomineral matrix of enamel apatite provides a large number of nucleation and deposition sites of L-Arginine functionalized nano-cHAP, which is favorable for coating formation. It is seen that the layer deposited on the surface of

the biotemplate repeats the characteristic microstructure of repeating blocks of prisms, mimicking the natural enamel morphology in the apatite track region.

Using low-angle X-ray diffraction, we obtained additional information on the crystalline state (phase composition, preferential orientation, and crystallinity) of PDA-based biomimetic layers deposited on biotemplate (natural enamel) and mineralized using nano-cHAP functionalized with the amino acid L-Arginine.

Figure 4a shows low-angle XRD scans of natural enamel (sample S5), enamel after application of one layer of PDA (sample S6<sub>1</sub>), and PDA-based biomimetic layer mineralized with nano-cHAP functionalized with the amino acid L-Arginine deposited on natural enamel (sample S8). The figure also shows diffraction from the nanocrystalline hydroxyapatite powder (nano-cHAP) used for synthesis and the nano-cHAP sample functionalized with the amino acid L-Arginine deposited onto the aluminum foil substrate.

The data analysis shows that XRD scans of samples contain a set of diffraction maxima, well corresponding to the main mineral phase in enamel composition—calcium hydroxyapatite (ICDD 01-074-0565). At the same time, changes in the ratio of intensities of diffraction peaks characteristic of stoichiometric hydroxyapatite are observed, which is associated with the presence of impurities and substitutions in the crystal lattice as well as texture due to the characteristic morphology of enamel in the shear region. It can be observed that pretreatment of enamel [etching in 38% orthophosphoric acid solution and in 12% calcium hydroxide ( $\text{Ca}(\text{OH})_2$ ) solution] and deposition of a single layer of PDA (sample S6<sub>1</sub>—enamel after deposition of one PDA nanolayer on its pretreated layer) lead to changes in the intensities of a number of diffraction peaks, which is a consequence of the removal of the upper smeared enamel layer formed during the preparation of the biotemplate. As a result of such pretreatment, nonuniform etching of the apatite crystals can take place when the crystals with a certain direction are etched more rapidly, thus leading to the texture effect.<sup>49</sup>

At the same time, an XRD scan (Figure 4a) of a PDA-based biomimetic layer mineralized with nano-cHAP functionalized with the amino acid L-Arginine deposited on natural enamel (sample S8) shows a significant increase in the intensity ratio of diffraction maxima (211) and (200) compared to natural

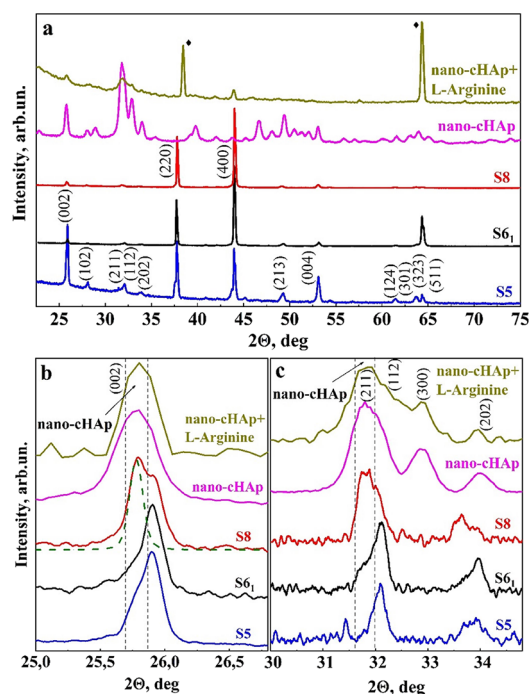


**Figure 4.** Low-angle XRD scans of samples of natural enamel (sample S5); enamel after application of one layer of PDA on its pretreated surface (sample S6<sub>1</sub>), biomimetic layer on natural enamel (sample S8); nanocrystalline hydroxyapatite powder (nano-cHAp); nano-cHAp sample functionalized with amino acid L-Arginine. (a) Overview diffraction; (b) scan in the region of (002) HAp reflex; (c) diffraction in the region of HAp main reflexes (211), (112), and (300). The diffraction in figure (a) is presented without normalization and in figures (b) and (c) with normalization. ◆—diffraction pattern from the aluminum foil substrate used for deposition of the nano-cHAp sample functionalized with amino acid L-Arginine.

enamel, also after preparation, indicating the deposition of nano-cHAp on the surface.<sup>50</sup> Comparative analysis shows that PDA promotes induction of hydroxyapatite crystal deposition on the enamel slice surface. At the same time, functionalization of nano-cHAp with the amino acid L-Arginine leads to redistribution of the intensity of the main hydroxyapatite reflexes and broadening of the (112) and (002) peaks (Figure 4b,c). This suggests that nano-cHAp hydroxyapatite nanocrystals are not randomly orientated, which is also a consequence of the decrease in the average size of HAp particles in biocomposites.<sup>50</sup>

At the same time as it was shown in our previous work,<sup>50</sup> where the features of the molecular structure in biomimetic composites comprising L-Arginine were studied, mechanisms of molecular orientation of this amino acid with carbonate-substituted hydroxyapatite take place in these systems. Thus, for the samples of biomimetic n-cHAp/L-Arginine composites, redistribution in the intensities of the main diffraction reflections of n-cHAp was observed, indicating the formation of the texture, i.e., directed agglomeration of hydroxyapatite in the sample.

Both facts probably support the occurrence of bonding of catecholamine groups in PDA coating with functionalized nano-cHAp, which can regulate the crystallographic orientation and crystallinity.<sup>51</sup> Meanwhile, crystallinity is known to be related to the degree of ordering and the size of hydroxyapatite crystals. Using X-ray diffraction results and the approach described in Sa et al.,<sup>52</sup> we calculated the crystallinity index  $C_1$

in a biomimetic layer and a natural enamel sample based on the fwhm of (002) reflection.

The results show that for natural enamel,  $C_1 \sim 1.3$ , and after applying one layer of PDA (sample S6<sub>1</sub>) to its pretreated surface,  $C_1 \sim 3.375$ . The significant increase in the crystallinity index is due to the removal of the smeared enamel layer. To calculate the CI of the biomimetic PDA layer mineralized using nano-cHAp functionalized with the amino acid L-Arginine, we extracted the (002) reflex from the total diffraction (see Figure 4b). The found crystallinity index of the biomimetic layer was  $C_1 \sim 6$ , indicating a high degree of mineralization of the layer formed on the enamel surface, as well as pointing to the regular and dense aggregation of nano-cHAp nanocrystals into larger crystals mimicking the morphology of natural enamel rods.

At the same time, we measured the value of microhardness of a slice of natural enamel (sample S5) without treatment and a sample of PDA-based biomimetic layer mineralized with nano-cHAp functionalized with the amino acid L-Arginine deposited on natural enamel (sample S8). It follows from the results that for natural enamel, this value takes the value  $HV \sim 306.8 \pm 9.5$ , while for the biomimetic layer (sample S8),  $HV \sim 290.8 \pm 7.9$ . It should be noted that the value of hardness of natural enamel found by us correlates well with the known literature data.<sup>53</sup> At the same time, the microhardness of the deposited biomimetic layer practically coincides with the microhardness of natural hard tissue.

It should be noted that the deposited organic mineral layers should correspond by their mechanical characteristics to the native dental enamel. In the case of a considerable microhardness increase, the mechanical destruction of the layer can take place under dynamic load, which affects enamel in real conditions. Therefore, in order to get practical use, it is necessary to achieve comparable mechanical properties for the obtained biomimetic layers. As was shown in our previous work,<sup>33</sup> deposition of the biomimetic layer based on hydroxyapatite (nano-cHAp) on the surface of native enamel in various conditions including codeposition with amino acids makes it possible to attain the greater values of microhardness due to the long-term deposition. The mechanisms of layer-by-layer deposition play a significant role in the reproduction of the hierarchical structure of enamel, formation of the ordered composite, and attainment of mechanical characteristics similar to those of the native enamel.

It has been previously demonstrated that the developed morphology of the substrate plays an important role in the deposition of mineralizing layers on biotemplates.<sup>19,29,33</sup> The enamel matrix used as a substrate has not only a specific morphology but also complex physical and chemical structural organization. At the same time, the quality of the deposited nanoscale PDA layer must inevitably affect its spectroscopic characteristics. Therefore, in order to establish the influence of local changes in the chemical environment on the biotemplate surface during the deposition of the PDA coating, to confirm the homogeneity of the layer and that it is deposited on enamel apatite crystals, we used IR *s*-SNOM near-field scanning optical microscopy. The involvement of broadband infrared radiation from a high-power quantum-cascade IR laser in the measurement scheme provided high spectral irradiance and allowed us to study spectral features with nanoscale spatial resolution (no worse than  $\sim 10$  nm). Considering the physical requirements of the IR *s*-SNOM method and the requirements for height variations, studies were performed on a sample of reference natural enamel (sample S5), as well as after the

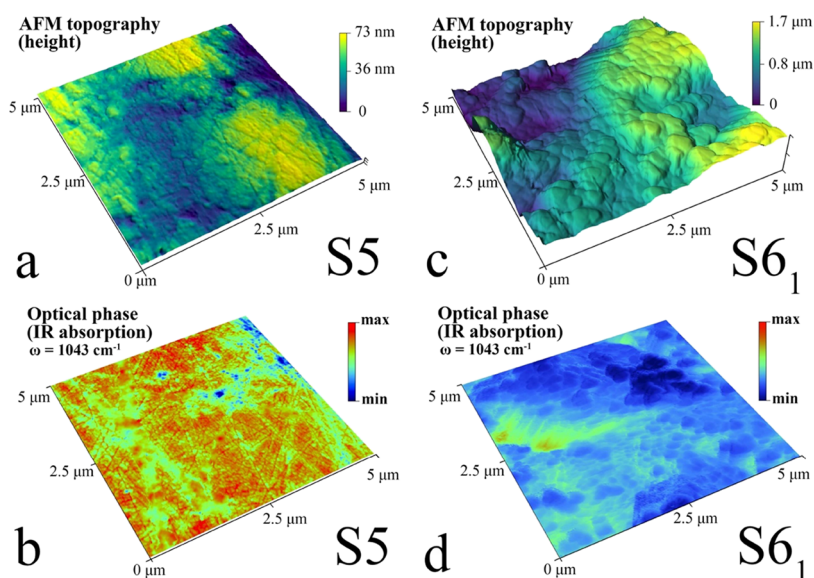


**Figure 5.**  $5 \times 5 \mu\text{m}^2$  AFM image of topology (a, c) and optical phase (b, d) for sample S5 (a, b) and sample S6, after applying the first layer of PDA (c, d).

application of the first PDA layer on the surface of the pretreated biotemplate (sample S6<sub>1</sub>).

To visualize the chemical contrast, near-field images of the s-SNOM optical phase were obtained simultaneously with the registration of the sample surface topology. For this purpose, the resonance photon energy corresponding to the frequency of  $1043 \text{ cm}^{-1}$  and coinciding with the characteristic vibrational mode  $\nu_3 \text{ PO}_4^{3-}$  in the IR spectrum of carbonate-substituted hydroxyapatite, the crystallochemical unit of the mineral component of human teeth, was chosen.<sup>54</sup>

A  $5 \mu\text{m} \times 5 \mu\text{m}$  AFM image of the surface topology of the reference natural enamel sample S5 is shown in Figure 5a. Despite the fine polishing, the typical core structure of the enamel is clearly visible, although residual polishing marks are observed. The chemical contrast showing the distribution of phosphate groups in this area and visualized with IR s-SNOM (Figure 5b) indicates a rather homogeneous (within the investigated area) presence of the mineral (phosphate) component. At the same time, based on the contrast, it can be observed that the regions with the maximum value of the optical phase, which is proportional to the optical absorption intensity  $\nu_3 \text{ PO}_4^{3-}$ , are localized in the areas that in the topology images correspond to the exit of enamel rods (Figure 5a,b).<sup>40,55</sup>

Analyzing the AFM image of the topology of sample S6 after deposition of the first PDA layer, it can be observed (Figure 5c, sample S6<sub>1</sub>) that because of enamel pretreatment its highly textured microstructure is clearly visible. The sample surface after deposition of the first PDA layer has a characteristic granular morphology, with quasi-planar areas, formed due to the pretreatment of the enamel using orthophosphoric acid and calcium hydroxide as well as the deposition of the PDA-based coating. The slope of the enamel apatite prisms visualized in the AFM topological image is a consequence of the specific shearing of the dental tissue (Figure 5c, sample S6<sub>1</sub>).

As for the chemical contrast plotted for sample S6 based on the distribution of the optical phase value, which corresponds to the infrared absorption of the phosphate group (Figure 3d, sample S6<sub>1</sub>), it is necessary to take into account the following

facts. Since the effective roughness of the useful signal output in the IR s-SNOM method is up to 100 nm,<sup>56</sup> the regions with minimal optical absorption on the map correspond to the maximum thickness of the deposited PDA layer (Figure 5c, sample S6<sub>1</sub>). Comparing simultaneously the topology and optical phase images for sample S6<sub>1</sub> (Figure 5c,d), it can be seen that the PDA film covers the practical entire surface of the sample, but its thickness is maximum on the surface of the existing enamel prisms.

It should be noted that the obtained result correlates with earlier works, where it was demonstrated that in the area of interprism space (organic matrix), although there was deposition of the polydopamine layer, but further remineralization in these zones was not great.<sup>57</sup> It was demonstrated that coating the enamel with a PDA layer could promote homogeneous nucleation of hydroxyapatite crystals in the enamel. In view of the homogeneity in the distribution of the PDA film over the enamel surface, as indicated by the chemical contrast associated with the uptake of phosphate groups, a similar result can be expected when PDA layers mineralized with nano-cHAp nanocrystals are deposited on the surface of biotemplates.

Further characterization of biomimetic layers based on nano-cHAp-amino acid-PDA was performed by using molecular IR and Raman microspectroscopy methods. Both methods allow for the study of chemical structures based on carbon materials formed due to van der Waals bonds and therefore were used among others to confirm the formation of polydopamine-based biomimetic layers. In Figure 6, the Raman spectra in the region from 200 to 2000  $\text{cm}^{-1}$  of samples in which PDA-based films were deposited on Si plates are shown.

As can be seen from the obtained data (Figure 6), in all spectra, the most intense mode is the oscillation located around 521  $\text{cm}^{-1}$ . This maximum belongs to the single-crystalline silicon substrate Si(111) and represents the TO optical phonon at the  $\Gamma$  point of the Brillouin zone. Also in the spectra of all samples, there is a mode in the region 920–990  $\text{cm}^{-1}$ , belonging to the 2(TA + TO) fluctuation of Si(111).

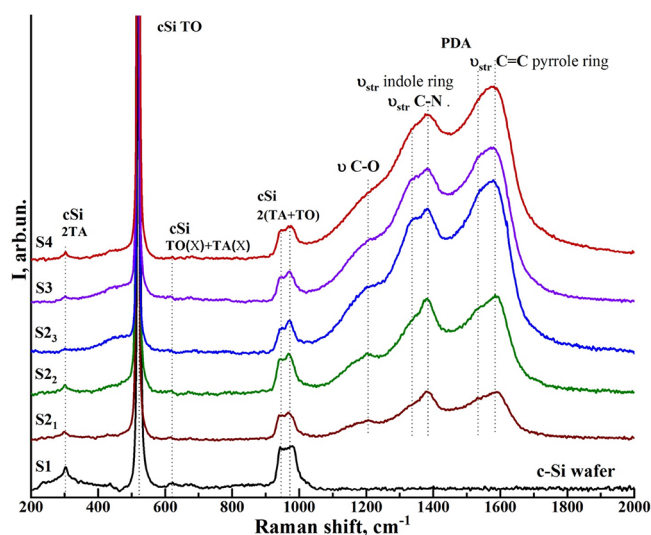


**Figure 6.** Raman spectra of samples S2–S4 as well as the silicon reference wafer (sample S1) used for the deposition of PDA layers.

The spectra of samples S2 to S4 in the region from 1200 to 1700  $\text{cm}^{-1}$  show broad characteristic bands, which are usually present in PDA-based films. Thus, the overlapping maxima around 1336–1382  $\text{cm}^{-1}$  are associated with indole ring stretching vibrations and C–N structure of polydopamine, while the peak around 1582  $\text{cm}^{-1}$  is attributed to C=C pyrrole ring stretching or associated with catechol ring strain vibrations.<sup>58</sup> As for the mode around 1205  $\text{cm}^{-1}$ , it is associated with stretching vibrations of C–O and C–O–C groups and residues in dopamine polymerization.<sup>28,59</sup> It should be noted that layer-by-layer deposition of PDA leads to an increase in the intensity of modes associated with polydopamine molecular groups (Figure 6, spectra of sample S2) after deposition of the first (S2<sub>1</sub>), second (S2<sub>2</sub>), and third (S2<sub>3</sub>) layers of PDA, respectively. The increasing thickness of the PDA coating correlates with the relative intensities of the PDA modes in the spectra. No other fluctuations are observed in the Raman spectra. In particular, the presence in the spectra of samples S3 and S4 of maxima attributed to vibrations of both amino acids L-Arginine and nano-chAp is not recorded. In the first case, they are superimposed as high-intensity modes of polydopamine, and in the second case, they are localized in the Si 2TO vibrational region. Considering the low concentration of L-Arginine and nano-chAp, we can observe only minor changes in the spectral profile of samples S3 to S4 (Figure 6), detected as a transformation of the bands assigned to PDA and Si 2TO. However, the comparison of all the recorded Raman spectra indicates the uniformity of the deposition mechanisms of the PDA-based film under the given technological conditions and the chosen type of substrate, regardless of its macromorphology and micromorphology.

Raman spectra of natural enamel (sample S5), as well as samples S6–S8, for which natural hard tissue (enamel) was chosen as a substrate, are presented in Figure 7. It follows from the results that the main high-intensity modes in all spectra belong to the characteristic vibrations of apatite in natural enamel. The most intense maximum around 960  $\text{cm}^{-1}$  is associated with the symmetric valence vibration  $\nu_1 \text{PO}_4^{3-}$ .<sup>3–62</sup> In the 420–450 and 580–620  $\text{cm}^{-1}$  region, there are  $\nu_2$  and  $\nu_4 \text{PO}_4^{3-}$  bending modes formed by two and four overlapping maxima, respectively.<sup>37</sup> In the range 1000–1100  $\text{cm}^{-1}$ , there

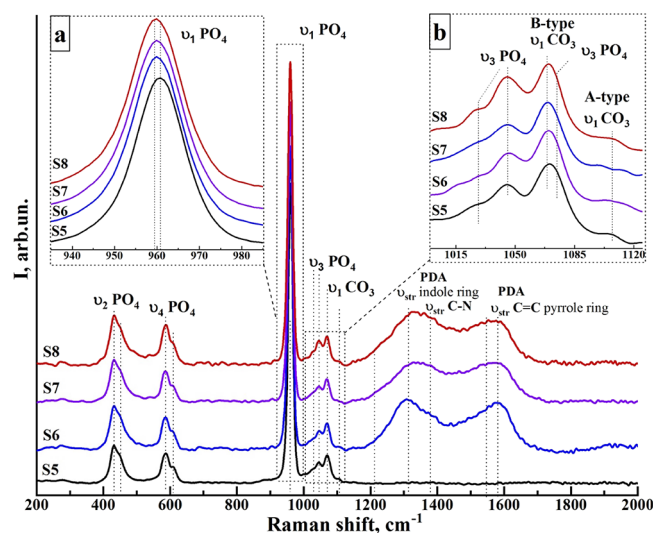


**Figure 7.** Raman spectra of samples S6–S8, for which PDA layers were deposited on the biotemplate (natural enamel), as well as the spectrum of the reference natural enamel sample (sample S5). The insets show (a) symmetric  $\nu_1 \text{PO}_4^{3-}$  valence vibrations; (b) the region of carbonate  $\nu_1 \text{CO}_3^{2-}$  and phosphate  $\nu_3 \text{PO}_4^{3-}$  vibrations.

are peaks correlated with  $\nu_3 \text{PO}_4^{3-}$  stretching mode, as well as a low-intensity feature around 1015  $\text{cm}^{-1}$  attributed to the  $\nu_4 \text{PO}_4^{3-}$  oscillation of the  $\text{HPO}_4$  group, which coincides with the known literature data.<sup>60,63,64</sup> The presence of natural enamel carbonate in the apatite composition is detected as a consequence of the occurrence of a low-intensity maximum around 1070–1075  $\text{cm}^{-1}$  in the Raman spectrum of sample S5 (Figure 7) associated with the  $\nu_1$  mode of  $\text{CO}_3^{2-}$  (B-type substitution).<sup>65</sup> In addition, in the 1050–1110  $\text{cm}^{-1}$  region of the same spectrum, there is a  $\nu_1 \text{CO}_3^{2-}$  (A-type substitution) oscillation, which is characteristic of biogenic materials.<sup>66–68</sup>

As in the case of samples on silicon wafers (S2–S4), deposition of PDA coatings on biotemplates leads to the appearance in Raman spectra (Figure 7) of two broad maxima associated with the indole ring and C–N vibrations near 1350  $\text{cm}^{-1}$  and C=C pyrrole ring stretching of the catechol ring near 1580  $\text{cm}^{-1}$ . Moreover, in contrast to the spectra of PDA layers deposited on silicon wafers (Figure 6), in the Raman spectra of biomimetic PDA films on natural enamel (Figure 7), the mode around 1205  $\text{cm}^{-1}$  attributed to stretching vibrations of C–O and C–O–C groups is less intense. Moreover, it is clearly visible that the performed procedure of mineralization of the PDA layer using nano-chAp (see Figure 7, sample S7) is not reflected in the change of the spectral profile, relative to the sample with a similarly deposited PDA layer (Figure 7, sample S6). On the contrary, the deposition of a biomimetic PDA layer mineralized using nano-chAp and functionalized with the amino acid L-Arginine (Figure 7, sample S8) leads to a redistribution of the intensity of the vibrations associated with PDA. Thus, the intensity of C=C pyrrole ring stretching of the catechol ring and H–N–C in-plane bending vibration<sup>69</sup> decreases relative to indole ring and C–N vibrations, which in turn may indicate the binding of DPA to nano-chAp.

At the same time, it should be noted that the performed biotemplate pretreatment procedure, as well as the deposition of PDA-layers of mineralized nano-chAp, led to a transformation of the IR spectral profile in the region of phosphate vibrations  $\nu_1 \text{PO}_4^{3-}$  980  $\text{cm}^{-1}$  and  $\nu_3 \text{PO}_4^{3-}$  1000–1110  $\text{cm}^{-1}$  (see Figure 7, insets a,b). The frequency shift toward lower



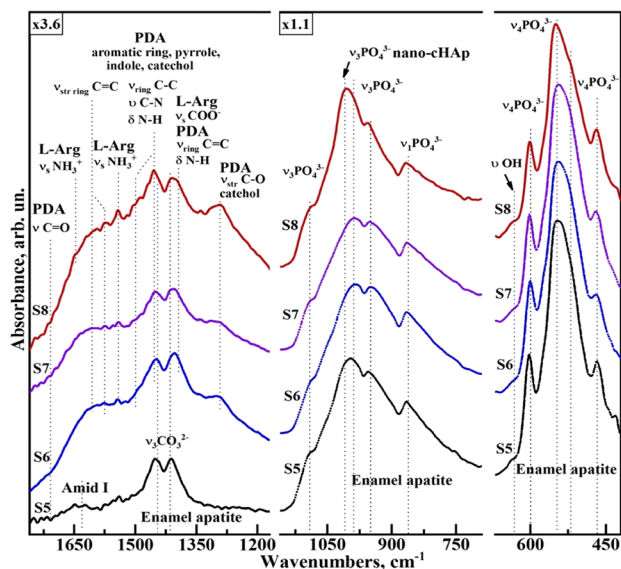


**Figure 9.** IR absorption spectra of samples S6–S8 for which PDA layers were deposited on the biotemplate (natural enamel) as well as the spectrum of the reference natural enamel sample (sample S5). The spectra are given with different scales on the intensity scale.

S6–S8, for which the biomimetic layers were similarly deposited using the technology developed by using silicon wafers (samples S2–S4). In view of the nanoscale thickness of the deposited layer, the IR spectra are presented in three bands in which the main vibrational modes attributed to the natural enamel and the biomimetic layer component are located. The spectra in Figure 9 are presented at different scales to visualize the changes in the profiles and the transformation and the spectral features present.

Analysis of the IR spectrum from healthy enamel (Figure 9, sample S5) shows that it contains maxima associated with vibrations of the mineral component of the enamel. The broad absorption band in the 1100–900  $\text{cm}^{-1}$  range represents the overlapping maxima of the  $\nu_3 \text{PO}_4^{3-}$  phosphate group vibrations. In the 960  $\text{cm}^{-1}$  area, a weak  $\nu_1 \text{PO}_4^{3-}$  (symmetric stretching) band is located in the IR spectrum of the enamel reference. In the 650–450  $\text{cm}^{-1}$  region, there is another intense absorption band, which is formed by four overlapping maxima, which are antisymmetric bending phosphate modes  $\nu_4 \text{PO}_4^{3-}$ . The presence in the composition of natural apatite enamel carbonate groups  $\text{CO}_3^{2-}$  is reflected in the form of active in the IR spectrum of sample S5 in the range of 1450–1410  $\text{cm}^{-1}$  antisymmetric stretching vibration mode  $\nu_3 \text{CO}_3^{2-}$ . This mode is characteristic of carbonate-substituted B-type hydroxyapatite when the phosphate anion  $\text{PO}_4^{3-}$  is substituted by the  $\text{CO}_3^{2-}$  group characteristic. As for the organic component of natural enamel, a weakly intense maximum attributed to Amid I is present in the spectrum of sample S5 in the region of 1625  $\text{cm}^{-1}$ .<sup>57</sup> Note that the experimental FTIR spectral profile of natural enamel is in excellent agreement with the literature data.<sup>54,80</sup>

In the spectra of samples S6–S8, in addition to the vibrations attributed to enamel apatite, features associated with chemical groups in the PDA composition appear, similar to those detected in the spectra of layers deposited on silicon wafers (Figure 8). However, a detailed analysis allows us to draw the following important conclusions. The deposition of the PDA layer on the biotemplate (sample S6) and the

mineralization of the PDA layer using nano-cHAp (sample S7) do not lead to a transformation of the spectral profile in the region of phosphate vibrations. However, features appear in the spectra (in the form of shoulders) around 1600 and 1270  $\text{cm}^{-1}$  associated with C=C stretching in the aromatic ring and C–O stretching in the catechol group PDA vibrations, respectively.<sup>81</sup> In addition, the spectrum of sample S7 registers low-intensity features that were previously detected in the spectrum of sample S4 and belong to the L-Arginine. It is noteworthy that in the spectrum of a PDA-based biomimetic layer deposited on natural enamel, mineralized using nano-cHAp and functionalized with the amino acid L-Arginine (Figure 9, sample S8), there is a significant increase in the intensity of the maximum in the region of 1470–1450  $\text{cm}^{-1}$ , which is attributed to the  $\nu_{\text{ring}}(\text{C}-\text{C}) + \nu(\text{C}-\text{N}) + \delta(\text{O}-\text{H})$  aliphatic  $\text{CH}_x$  indole ring of PDA.<sup>81</sup> This indicates that PDA can interact with an amino acid without changing its basic structure, similar to what was demonstrated in the article by Yanan Qu et al. in the case of interaction between PDA and collagen.<sup>23</sup>

In addition, deposition of a biomimetic PDA layer mineralized with nano-cHAp and functionalized with the amino acid L-Arginine on natural enamel results in a high-frequency shift of the  $\nu_1$ ,  $\nu_3$ , and  $\nu_4 \text{PO}_4^{3-}$  phosphate modes in the IR spectra (sample S8) relative to their position in the spectrum of healthy enamel (sample S5) and the spectra of samples S6 and S7 (see Figure 9). In addition, in the IR spectrum of sample S8, the peaks attributed to polydopamine are much more pronounced. This is due to the effect of the amino acid on carbonate-substituted hydroxyapatite, which was used to mineralize the PDA layer, resulting in the mutual orientation of L-Arginine and nano-cHAp molecules. The resulting ordering (orientation) of nano-cHAp crystals in the mineralized PDA layer is spectrally reflected in the form of a frequency shift as well as in the transformation of the profile of phosphate modes similar to what is registered for different regions of natural enamel with the specific orientation of apatite prisms.<sup>82</sup>

It should be noted, earlier Koutsopoulos S. and Dalas E.<sup>83</sup> and many others<sup>10,11,18</sup> showed that the presence of an amino acid in the supersaturated solution used for mineralization changes the growth rate of HAp crystals. The presence of a foreign compound in the supersaturated solution from which crystallization occurs will cause the dissolved nanoparticles to interact with the surface of the deposited PDA film.<sup>18</sup> Since amino acids have active functional groups (carboxyl and/or amino groups), they can be reversibly adsorbed on the crystal surface where the centers of positively and negatively charged ions are located.<sup>34,50</sup> For the same reason, amino acid-functionalized hydroxyapatite nanocrystals can be located on the surface of the PDA layer during PDA layer deposition, since adsorption of inhibitor molecules at active growth centers can prevent their incorporation into the crystal lattice of the matrix.<sup>83</sup> In this case, L-arginine acts as a conjunction agent by binding to the surface of the PDA layer and simultaneously to  $\text{Ca}^{2+}$  и  $\text{PO}_4^{3-}$  ions of hydroxyapatite nanocrystals.<sup>11,18,27,76</sup> At the same time, as was shown earlier,<sup>21,57</sup> binding of the PDA-biomimetic layer to the pretreated enamel surface will promote the formation of hydroxyapatite nanocrystal packing, which is confirmed by IR-spectroscopy data. In the future, all of this should contribute to homogeneous nucleation of subsequent apatite-like layers at the stages of biomimetic remineralization.

Summarizing the results of the work done, it should be noted that the formation of homogeneous biomimetic mineralizing coatings on the surface of natural enamel can be realized based on accelerated deposition of layers of nature-like adhesive (polydopamine) mineralized with nanocrystals of carbonate-substituted hydroxyapatite (nano-cHAp) and functionalized with amino acid L-Arginine. Experiments performed in this work show that the proposed technique allows for the deposition of a quasi-planar layer covering practically the entire surface of the sample, regardless of the macromorphology and micromorphology of the template. The technique can be scaled and adapted to different substrates, taking into account the required thickness of the deposited PDA layers and their number.

However, it is impossible to cover a number of issues within the framework of this work, so in the future, our attention will be focused on the research of the interface between the biomimetic layer and natural hard tissue and optimization of technology to obtain mechanically and thermally resistant coatings with stable thickness.

#### 4. CONCLUSIONS

In our work, we have perfected a technology for accelerated deposition on silicon wafers and natural enamel slices (biotemplates) of biomimetic composite films based on polydopamine (PDA) and nanocrystalline carbonate-substituted hydroxyapatite (nano-cHAp) functionalized with the amino acid L-Arginine.

Using atomic force microscopy and IR s-SNOM near-field infrared scanning optical microscopy with nanoscale spatial resolution, the film morphology was studied, and the influence of local changes in the chemical environment on the biotemplate surface during deposition of the bioinspired coating was established. It was found that using the proposed technology, after deposition of the first PDA layer, the film formed on the enamel surface covers practically the entire surface of the specimen, and its thickness is maximum on the surface of the exiting enamel prisms. PDA induces the deposition of hydroxyapatite crystals on the enamel surface. At the same time, functionalization of nano-cHAp with the amino acid L-Arginine regulates the crystallographic orientation of HAp particles in the biomimetic layer, as well as the crystallinity of the mineralized layer.<sup>50</sup>

Calculation of the crystallinity index for the biomimetic layer showed a multiple increase compared to natural enamel. This indicates regular and dense aggregation of nano-cHAp into larger crystals imitating the morphology of natural enamel rods. The microhardness of the formed PDA-based biomimetic layer mineralized with nano-cHAp functionalized with the amino acid L-Arginine deposited on natural enamel was practically the same as that of natural enamel.

Characterization of nano-cHAp-amino acid PDA layers using molecular infrared and Raman microspectroscopy showed that L-arginine acts as a conjunction agent in the formation of biomimetic composite mineralized coatings. The uniformity of the mechanisms of PDA layer formation under different deposition conditions and substrate types allows the coating to be formed regardless of the macromorphology and micromorphology of the template.

However, in the future, our attention will focus on research of the interface between the biomimetic layer and natural hard tissue and optimization of the technology to obtain

mechanically and thermally resistant coatings with a stable thickness.

#### AUTHOR INFORMATION

##### Corresponding Author

Pavel Seredin – Voronezh State University, Voronezh 394018, Russia; [orcid.org/0000-0002-6724-0063](https://orcid.org/0000-0002-6724-0063); Email: [paul@phys.vsu.ru](mailto:paul@phys.vsu.ru)

##### Authors

Dmitry Goloshchapov – Voronezh State University, Voronezh 394018, Russia

Anna Emelyanova – Voronezh State University, Voronezh 394018, Russia

Konstantin Ereemeev – Voronezh State University, Voronezh 394018, Russia

Yaroslav Peshkov – Voronezh State University, Voronezh 394018, Russia

Khidmet Shikhaliev – Voronezh State University, Voronezh 394018, Russia

Andrey Potapov – Voronezh State University, Voronezh 394018, Russia

Yury Ippolitov – Department of Pediatric Dentistry with Orthodontia, Voronezh State Medical University, Voronezh 394006, Russia

Vladimir Kashkarov – Voronezh State University, Voronezh 394018, Russia

Dmitry Nesterov – Voronezh State University, Voronezh 394018, Russia

Kirill Shapiro – Voronezh State University, Voronezh 394018, Russia

Raul O. Freitas – Brazilian Synchrotron Light Laboratory (LNLS), Brazilian Center for Research in Energy and Materials (CNPEM), Campinas 13083-970 Sao Paulo, Brazil; [orcid.org/0000-0002-3285-5447](https://orcid.org/0000-0002-3285-5447)

Iman. A. Mahdy – Physics Department, Faculty of Science (Girls), Al-Azhar University, 11754 Cairo, Egypt

Complete contact information is available at:

<https://pubs.acs.org/10.1021/acsomega.3c08491>

##### Funding

This work was supported by the grant of Russian Science Foundation, grant number 21-75-10005.

##### Notes

The authors declare no competing financial interest.

The study was conducted according to the guidelines of the Declaration of Helsinki and approved by the Institutional Review Board (protocol number: Pr-002.003.2022, 3 March 2022).

#### ACKNOWLEDGMENTS

This research used the IMBUA beamline and the Microscopic Samples Laboratory (LAM) of the Brazilian Synchrotron Light Laboratory (LNLS) in the Brazilian Center for Research in Energy and Materials (CNPEM) through the beamtime proposal 20221588. Raul de Oliveira Freitas acknowledges the funding agencies for supporting the research under the grants FAPESP 2019/14017-9, 2022/11987-0, 2021/10487-0, and CNPq 309946/2021-2. Access to scientific equipment and methodology was provided under the support of the Ministry of Science and Higher Education of Russia, Agreement N 075-15-2021-1351.

## REFERENCES

- (1) Cai, S.; Cheng, Y.; Qiu, C.; Liu, G.; Chu, C. The Versatile Applications of Polydopamine in Regenerative Medicine: Progress and Challenges. *Smart Mater. Med.* **2023**, *4*, 294–312.
- (2) Singer, L.; Fouda, A.; Bourauel, C. Biomimetic Approaches and Materials in Restorative and Regenerative Dentistry: Review Article. *BMC Oral Health* **2023**, *23* (1), 105.
- (3) Zhao, H.; Liu, S.; Lu, J.; Yang, X.; Yang, Z.; Li, F.; Guo, L. Natural Tooth Enamel and Its Analogs. *Cell Rep. Phys. Sci.* **2022**, *3* (7), No. 100945.
- (4) Šupová, M. The Significance and Utilisation of Biomimetic and Bioinspired Strategies in the Field of Biomedical Material Engineering: The Case of Calcium Phosphat—Protein Template Constructs. *Materials* **2020**, *13* (2), 327.
- (5) Zhang, Y. Y.; Li, Q. L.; Wong, H. M. Cell-Free Biomimetic Mineralization Strategies to Regenerate the Enamel Microstructure. *Crystals* **2021**, *11* (11), 1385.
- (6) Kuczumow, A.; Gorzelak, M.; Kosiński, J.; Lasota, A.; Blicharski, T.; Gaęala, J.; Nowak, J.; Jarzębski, M.; Jabłoński, M. Hierarchy of Bioapatites. *Int. J. Mol. Sci.* **2022**, *23* (17), 9537.
- (7) DeRocher, K. A.; Smeets, P. J. M.; Goodge, B. H.; Zachman, M. J.; Balachandran, P. V.; Stegbauer, L.; Cohen, M. J.; Gordon, L. M.; Rondinelli, J. M.; Kourkoutis, L. F.; Joester, D. Chemical Gradients in Human Enamel Crystallites. *Nature* **2020**, *583* (7814), 66–71.
- (8) Wegst, U. G. K.; Bai, H.; Saiz, E.; Tomsia, A. P.; Ritchie, R. O. Bioinspired Structural Materials. *Nat. Mater.* **2015**, *14* (1), 23–36.
- (9) Ding, Y.; Cai, M.; Niu, P.; Zhang, H.; Zhang, S.-Q.; Sun, Y. Ultrashort Peptides Induce Biomimetic Mineralization. *Compos. Part B Eng.* **2022**, *244*, No. 110196.
- (10) Erceg, I.; Maltar-Strmečki, N.; Jurašin, D. D.; Strasser, V.; Čurlin, M.; Lyons, D. M.; Radatović, B.; Mlinarić, N. M.; Kralj, D.; Sikirić, M. D. Comparison of the Effect of the Amino Acids on Spontaneous Formation and Transformation of Calcium Phosphates. *Crystals* **2021**, *11* (7), 792.
- (11) Li, Z.; Ren, Q.; Cui, J.; Hu, D.; Tian, T.; He, T.; Wang, K.; Jiang, W.; Zhang, L. Comparing the Efficacy of Hydroxyapatite Nucleation Regulated by Amino Acids, Poly-Amino Acids and an Amelogenin-Derived Peptide. *CrystEngComm* **2020**, *22* (22), 3814–3823.
- (12) Yanyan, S.; Guangxin, W.; Guoqing, S.; Yaming, W.; Wuhui, L.; Osaka, A. Effects of Amino Acids on Conversion of Calcium Carbonate to Hydroxyapatite. *RSC Adv.* **2020**, *10* (61), 37005–37013.
- (13) Lyu, D.; Zhang, Q.; Wu, Y.; Chen, L.; Li, X.; Ren, H.; Yan, Y. Effects of Particle Size of Hydroxyapatite on Mechanical Property and Cytocompatibility of Hydroxyapatite/Poly(Amino Acid) Composites. *Polym. Compos.* **2022**, *43* (2), 1107–1120.
- (14) Comeau, P.; Willett, T. Impact of Side Chain Polarity on Non-Stoichiometric Nano-Hydroxyapatite Surface Functionalization with Amino Acids. *Sci. Rep.* **2018**, *8* (1), 12700.
- (15) Bijle, M. N.; Pichika, M. R.; Mak, K.-K.; Parolia, A.; Babar, M. G.; Yiu, C.; Daood, U. Concentration-Dependent Multi-Potentiality of L-Arginine: Antimicrobial Effect, Hydroxyapatite Stability, and MMPs Inhibition. *Molecules* **2021**, *26* (21), 6605.
- (16) Saranya, S.; Samuel Justin, S. J.; Vijay Solomon, R.; Wilson, P. L-Arginine Directed and Ultrasonically Aided Growth of Nanocrystalline Hydroxyapatite Particles with Tunable Morphology. *Colloids Surf. Physicochem. Eng. Asp.* **2018**, *538*, 270–279.
- (17) Goloshchapov, D.; Kashkarov, V.; Nikitkov, K.; Bartenev, V.; Ippolitov, I.; Ippolitov, Y.; Seredin, P. Study of the Impact of Amino Acids Hydrochloride Forms on the Formation of Biomimetic Composites in the Presence of Nanocrystalline Hydroxyapatite. *J. Phys. Conf. Ser.* **2020**, *1697* (1), No. 012040.
- (18) Tavafoghi, M.; Cerruti, M. The Role of Amino Acids in Hydroxyapatite Mineralization. *J. R. Soc. Interface* **2016**, *13* (123), 20160462.
- (19) Shao, C.; Jin, B.; Mu, Z.; Lu, H.; Zhao, Y.; Wu, Z.; Yan, L.; Zhang, Z.; Zhou, Y.; Pan, H.; Liu, Z.; Tang, R. Repair of Tooth Enamel by a Biomimetic Mineralization Frontier Ensuring Epitaxial Growth. *Sci. Adv.* **2019**, *5* (8), No. eaaw9569.
- (20) Teng, R.; Meng, Y.; Zhao, X.; Liu, J.; Ding, R.; Cheng, Y.; Zhang, Y.; Zhang, Y.; Pei, D.; Li, A. Combination of Polydopamine Coating and Plasma Pretreatment to Improve Bond Ability Between PEEK and Primary Teeth. *Front. Bioeng. Biotechnol.* **2021**, *8*, No. 630094.
- (21) Kaushik, N.; Nhat Nguyen, L.; Kim, J. H.; Choi, E. H.; Kumar Kaushik, N. Strategies for Using Polydopamine to Induce Biomimetic Mineralization of Hydroxyapatite on Implant Materials for Bone Tissue Engineering. *Int. J. Mol. Sci.* **2020**, *21* (18), 6544.
- (22) Bogdan, D.; Grosu, I.-G.; Filip, C. How Thick, Uniform and Smooth Are the Polydopamine Coating Layers Obtained under Different Oxidation Conditions? An in-Depth AFM Study. *Appl. Surf. Sci.* **2022**, *597*, No. 153680.
- (23) Qu, Y.; Gu, T.; Du, Q.; Shao, C.; Wang, J.; Jin, B.; Kong, W.; Sun, J.; Chen, C.; Pan, H.; Tang, R.; Gu, X. Polydopamine Promotes Dentin Remineralization via Interfacial Control. *ACS Biomater. Sci. Eng.* **2020**, *6* (6), 3327–3334.
- (24) Seredin, P.; Goloshchapov, D.; Buylov, N.; Kashkarov, V.; Shikhaliev, K.; Potapov, A.; Ippolitov, Y.; Kartsev, V.; Kuyumchyan, S.; De Oliveira Freitas, R. A Study of the Peculiarities of the Formation of a Hybrid Interface Based on Polydopamine between Dental Tissues and Dental Composites, Using IR and Raman Microspectroscopy, at the Submicron Level. *Int. J. Mol. Sci.* **2023**, *24* (14), 11636.
- (25) Jia, L.; Han, F.; Wang, H.; Zhu, C.; Guo, Q.; Li, J.; Zhao, Z.; Zhang, Q.; Zhu, X.; Li, B. Polydopamine-Assisted Surface Modification for Orthopaedic Implants. *J. Orthop. Transl.* **2019**, *17*, 82–95.
- (26) Yan, L.; Zheng, C.; Yuan, D.; Guo, Z.; Cui, Y.; Xie, Z.; Chen, Z.; Tang, R.; Liu, Z. Fast Construction of Biomimetic Organic–Inorganic Interface by Crosslinking of Calcium Phosphate Oligomers: A Strategy for Instant Regeneration of Hard Tissue. *Adv. Healthc. Mater.* **2022**, *11* (23), 2201161.
- (27) Saranya, S.; Justin, S. J. S.; Edwin, N.; Wilson, P. Morphology and Functionalization Dependent Sensing of Dopamine on L-Arginine Functionalized Hydroxyapatite Nanoparticles. *ChemistrySelect* **2022**, *7* (26), No. e202201542.
- (28) Jumat, M. A.; Chevallier, P.; Mantovani, D.; Saidin, S. Everolimus Immobilisation Using Polydopamine Intermediate Layer on Poly(L-Lactic Acid)/Poly(D-Lactic Acid) Scaffold for Sustainable Anti-Proliferative Drug Release. *Mater. Today Commun.* **2022**, *31*, No. 103720.
- (29) El Gezawi, M.; Wöflle, U. C.; Haridy, R.; Fliefel, R.; Kaisarly, D. Remineralization, Regeneration, and Repair of Natural Tooth Structure: Influences on the Future of Restorative Dentistry Practice. *ACS Biomater. Sci. Eng.* **2019**, *5* (10), 4899–4919.
- (30) Wong, H. M.; Zhang, Y. Y.; Li, Q. L. An Enamel-Inspired Bioactive Material with Multiscale Structure and Antibacterial Adhesion Property. *Bioact. Mater.* **2022**, *7*, 491–503.
- (31) Mukherjee, K.; Ruan, Q.; Nutt, S.; Tao, J.; De Yoreo, J. J.; Moradian-Oldak, J. Peptide-Based Bioinspired Approach to Regrowing Multilayered Aprismatic Enamel. *ACS Omega* **2018**, *3* (3), 2546–2557.
- (32) Zhang, C.; Ou, Y.; Lei, W.-X.; Wan, L.-S.; Ji, J.; Xu, Z.-K. CuSO<sub>4</sub>/H<sub>2</sub>O<sub>2</sub>-Induced Rapid Deposition of Polydopamine Coatings with High Uniformity and Enhanced Stability. *Angew. Chem., Int. Ed.* **2016**, *55* (9), 3054–3057.
- (33) Seredin, P.; Goloshchapov, D.; Kashkarov, V.; Emelyanova, A.; Buylov, N.; Barkov, K.; Ippolitov, Y.; Khmelevskaia, T.; Mahdy, I. A.; Mahdy, M. A.; Prutskij, T. Biomimetic Mineralization of Tooth Enamel Using Nanocrystalline Hydroxyapatite under Various Dental Surface Pretreatment Conditions. *Biomimetics* **2022**, *7* (3), 111.
- (34) Goloshchapov, D. L.; Ippolitov, Yu. A.; Seredin, P. V. Mechanism of Interaction among Nanocrystalline Carbonate-Substituted Hydroxyapatite and Polar Amino-Acids for the Biomimetic Composite Technology: Spectroscopic and Structural Study. *Results Phys.* **2020**, *18*, No. 103277.

- (35) Goloshchapov, D. L.; Lenshin, A. S.; Savchenko, D. V.; Seredin, P. V. Importance of Defect Nanocrystalline Calcium Hydroxyapatite Characteristics for Developing the Dental Biomimetic Composites. *Results Phys.* **2019**, *13*, No. 102158.
- (36) Goloshchapov, D. L.; Gushchin, M. S.; Kashkarov, V. M.; Seredin, P. V.; Ippolitov, Y. A.; Khmelevsky, N. O.; Aksenenko, A. Yu. XPS and XANES Studies of Biomimetic Composites Based on B-Type Nano-Hydroxyapatite. *Results Phys.* **2018**, *9*, 1386–1387.
- (37) Goloshchapov, D.; Buylov, N.; Emelyanova, A.; Ippolitov, I.; Ippolitov, Y.; Kashkarov, V.; Khudyakov, Y.; Nikitkov, K.; Seredin, P. Raman and XANES Spectroscopic Study of the Influence of Coordination Atomic and Molecular Environments in Biomimetic Composite Materials Integrated with Dental Tissue. *Nanomaterials* **2021**, *11* (11), 3099.
- (38) Nakayama, M.; Kajiyama, S.; Kumamoto, A.; Nishimura, T.; Ikuhara, Y.; Yamato, M.; Kato, T. Stimuli-Responsive Hydroxyapatite Liquid Crystal with Macroscopically Controllable Ordering and Magneto-Optical Functions. *Nat. Commun.* **2018**, *9* (1), 568.
- (39) Ponzio, F.; Barthès, J.; Bour, J.; Michel, M.; Bertani, P.; Hemmerlé, J.; d'Ischia, M.; Ball, V. Oxidant Control of Polydopamine Surface Chemistry in Acids: A Mechanism-Based Entry to Superhydrophilic-Superoleophobic Coatings. *Chem. Mater.* **2016**, *28* (13), 4697–4705.
- (40) Beniash, E.; Stifler, C. A.; Sun, C.-Y.; Jung, G. S.; Qin, Z.; Buehler, M. J.; Gilbert, P. U. P. A. The Hidden Structure of Human Enamel. *Nat. Commun.* **2019**, *10* (1), 4383.
- (41) Seredin, P.; Goloshchapov, D.; Kashkarov, V.; Khudyakov, Y.; Ippolitov, I.; Ippolitov, Y.; Vongsvivut, J. Biomimetic Nano-c-HAP Hybrid Layer Engineering and Determination of Mechanisms of Its Integration with Native Hard Dental Tissue. *Results Eng.* **2021**, *11*, No. 100266.
- (42) Ocelic, N.; Huber, A.; Hillenbrand, R. Pseudoheterodyne Detection for Background-Free near-Field Spectroscopy. *Appl. Phys. Lett.* **2006**, *89* (10), No. 101124.
- (43) Keilmann, F.; Hillenbrand, R. Near-Field Microscopy by Elastic Light Scattering from a Tip. *Philos. Trans. R. Soc. London Ser. Math. Phys. Eng. Sci.* **1817**, 2004 (362), 787–805.
- (44) Zhou, Y.; Yang, Y.; Liu, R.; Zhou, Q.; Lu, H.; Zhang, W. Research Progress of Polydopamine Hydrogel in the Prevention and Treatment of Oral Diseases. *Int. J. Nanomedicine* **2023**, *18*, 2623–2645.
- (45) Zhang, J.; He, X.; Yu, S.; Zhu, J.; Wang, H.; Tian, Z.; Zhu, S.; Cui, Z. A Novel Dental Adhesive Containing Ag/Polydopamine-Modified HA Fillers with Both Antibacterial and Mineralization Properties. *J. Dent.* **2021**, *111*, No. 103710.
- (46) Coy, E.; Iatsunskyi, I.; Colmenares, J. C.; Kim, Y.; Mrówczyński, R. Polydopamine Films with 2D-like Layered Structure and High Mechanical Resilience. *ACS Appl. Mater. Interfaces* **2021**, *13* (19), 23113–23120.
- (47) Zhou, P.; Deng, Y.; Lyu, B.; Zhang, R.; Zhang, H.; Ma, H.; Lyu, Y.; Wei, S. Rapidly-Deposited Polydopamine Coating via High Temperature and Vigorous Stirring: Formation, Characterization and Biofunctional Evaluation. *PLoS One* **2014**, *9* (11), No. e113087.
- (48) Wu, G.; Li, J.; Qu, X.; Zhang, Y.; Hong, H.; Liu, C. Template Size Matched Film Thickness for Effectively in Situ Surface Imprinting: A Model Study of Glycoprotein Imprints. *RSC Adv.* **2015**, *5* (58), 47010–47021.
- (49) Dorozhkin, S. V. Dissolution Mechanism of Calcium Apatites in Acids: A Review of Literature. *World J. Methodol.* **2012**, *2* (1), 1.
- (50) Goloshchapov, D.; Kashkarov, V.; Nikitkov, K.; Seredin, P. Investigation of the Effect of Nanocrystalline Calcium Carbonate-Substituted Hydroxyapatite and L-Lysine and L-Arginine Surface Interactions on the Molecular Properties of Dental Biomimetic Composites. *Biomimetics* **2021**, *6* (4), 70.
- (51) Jin-Mei, X.; Xin-Ling, L.; Yan-Feng, G. Effect of Dopamine on Hydroxyapatite Deposition for Dental Restoration. *J. Inorg. Mater.* **2016**, *31* (1), 95.
- (52) Sa, Y.; Guo, Y.; Feng, X.; Wang, M.; Li, P.; Gao, Y.; Yang, X.; Jiang, T. Are Different Crystallinity-Index-Calculating Methods of Hydroxyapatite Efficient and Consistent? *New J. Chem.* **2017**, *41* (13), 5723–5731.
- (53) Chun, K.; Choi, H.; Lee, J. Comparison of Mechanical Property and Role between Enamel and Dentin in the Human Teeth. *J. Dent. Biomech.* **2014**, *5*, No. 1758736014520809.
- (54) Seredin, P.; Goloshchapov, D.; Ippolitov, Y.; Vongsvivut, J. Development of a New Approach to Diagnosis of the Early Fluorosis Forms by Means of FTIR and Raman Microspectroscopy. *Sci. Rep.* **2020**, *10* (1), 20891.
- (55) Seredin, P.; Goloshchapov, D.; Emelyanova, A.; Buylov, N.; Kashkarov, V.; Lukin, A.; Ippolitov, Y.; Khmelevskaia, T.; Mahdy, I. A.; Mahdy, M. A. Engineering of Biomimetic Mineralized Layer Formed on the Surface of Natural Dental Enamel. *Results Eng.* **2022**, *15*, No. 100583.
- (56) Muller, E. A.; Pollard, B.; Bechtel, H. A.; Van Blerkom, P.; Raschke, M. B. Infrared Vibrational Nanocrystallography and Nanoimaging. *Sci. Adv.* **2016**, *2* (10), No. e1601006.
- (57) Zhou, Y.-Z.; Cao, Y.; Liu, W.; Chu, C. H.; Li, Q.-L. Polydopamine-Induced Tooth Remineralization. *ACS Appl. Mater. Interfaces* **2012**, *4* (12), 6901–6910.
- (58) Felfel, R. M.; Parsons, A. J.; Chen, M.; Stuart, B. W.; Wadge, M. D.; Grant, D. M. Water Resistant Fibre/Matrix Interface in a Degradable Composite: Synergistic Effects of Heat Treatment and Polydopamine Coating. *Compos. Part Appl. Sci. Manuf.* **2021**, *146*, No. 106415.
- (59) Kumar, M.; Sreedhar, N.; Thomas, N.; Mavukkandy, M.; Ismail, R. A.; Aminabhavi, T. M.; Arafat, H. A. Polydopamine-Coated Graphene Oxide Nanosheets Embedded in Sulfonated Poly(Ether Sulfone) Hybrid UF Membranes with Superior Antifouling Properties for Water Treatment. *Chem. Eng. J.* **2022**, *433*, No. 133526.
- (60) Zelic, K.; Milovanovic, P.; Rakocevic, Z.; Askrabic, S.; Potocnik, J.; Popovic, M.; Djuric, M. Nano-Structural and Compositional Basis of Devitalized Tooth Fragility. *Dent. Mater. Off. Publ. Acad. Dent. Mater.* **2014**, *30* (5), 476–486.
- (61) Bērziņš, K.; Sutton, J. J.; Loch, C.; Beckett, D.; Wheeler, B. J.; Drummond, B. K.; Fraser-Miller, S. J.; Gordon, K. C. Application of Low-wavenumber Raman Spectroscopy to the Analysis of Human Teeth. *J. Raman Spectrosc.* **2019**, *50* (10), 1375–1387.
- (62) Pezzotti, G.; Zhu, W.; Boffelli, M.; Adachi, T.; Ichioka, H.; Yamamoto, T.; Marunaka, Y.; Kanamura, N. Vibrational Algorithms for Quantitative Crystallographic Analyses of Hydroxyapatite-Based Biomaterials: I, Theoretical Foundations. *Anal. Bioanal. Chem.* **2015**, *407* (12), 3325–3342.
- (63) Crane, N. J.; Popescu, V.; Morris, M. D.; Steenhuis, P.; Ignelzi, M. A., Jr. Raman Spectroscopic Evidence for Octacalcium Phosphate and Other Transient Mineral Species Deposited during Intra-membranous Mineralization. *Bone* **2006**, *39* (3), 434–442.
- (64) Stammeier, J. A.; Purgstaller, B.; Hippler, D.; Mavromatis, V.; Dietzel, M. In-Situ Raman Spectroscopy of Amorphous Calcium Phosphate to Crystalline Hydroxyapatite Transformation. *MethodsX* **2018**, *5*, 1241–1250.
- (65) Seredin, P.; Goloshchapov, D.; Buylov, N.; Kashkarov, V.; Emelyanova, A.; Ereemeev, K.; Ippolitov, Y. Compositional Analysis of the Dental Biomimetic Hybrid Nanomaterials Based on Bioinspired Nonstoichiometric Hydroxyapatite with Small Deviations in the Carbonate Incorporation. *Nanomaterials* **2022**, *12* (24), 4453.
- (66) Spizzirri, P. G.; Cochrane, N. J.; Prawer, S.; Reynolds, E. C. A Comparative Study of Carbonate Determination in Human Teeth Using Raman Spectroscopy. *Caries Res.* **2012**, *46* (4), 353–360.
- (67) Jegova, G.; Titorenkova, R.; Rashkova, M.; Mihailova, B. Raman and IR Reflection Micro-Spectroscopic Study of Er:YAG Laser Treated Permanent and Deciduous Human Teeth. *J. Raman Spectrosc.* **2013**, *44* (11), 1483–1490.
- (68) Penel, G.; Leroy, G.; Rey, C.; Bres, E. MicroRaman Spectral Study of the PO<sub>4</sub> and CO<sub>3</sub> Vibrational Modes in Synthetic and Biological Apatites. *Calcif. Tissue Int.* **1998**, *63* (6), 475–481.
- (69) Feng, J.; Fan, H.; Zha, D.; Wang, L.; Jin, Z. Characterizations of the Formation of Polydopamine-Coated Halloysite Nanotubes in Various pH Environments. *Langmuir* **2016**, *32* (40), 10377–10386.

- (70) Kopani, M.; Mikula, M.; Takahashi, M.; Rusnák, J.; Pinčík, E. FT IR Spectroscopy of Silicon Oxide Layers Prepared with Perchloric Acid. *Appl. Surf. Sci.* **2013**, *269*, 106–109.
- (71) Zangmeister, R. A.; Morris, T. A.; Tarlov, M. J. Characterization of Polydopamine Thin Films Deposited at Short Times by Autoxidation of Dopamine. *Langmuir* **2013**, *29* (27), 8619–8628.
- (72) Cai, G.; Hou, J.; Jiang, D.; Dong, Z. Polydopamine-Wrapped Carbon Nanotubes to Improve the Corrosion Barrier of Polyurethane Coating. *RSC Adv.* **2018**, *8* (42), 23727–23741.
- (73) Steeves, A. J.; Atwal, A.; Schock, S. C.; Variola, F. Evaluation of the Direct Effects of Poly(Dopamine) on the in Vitro Response of Human Osteoblastic Cells. *J. Mater. Chem. B* **2016**, *4* (18), 3145–3156.
- (74) Nejman, A.; Baranowska-Korczyk, A.; Ranoszek-Soliwoda, K.; Jasińska, I.; Celichowski, G.; Cieślak, M. Silver Nanowires and Silanes in Hybrid Functionalization of Aramid Fabrics. *Molecules* **2022**, *27* (6), 1952.
- (75) Xu, X.; Li, M.; Liu, Q.; Jia, Z.; Shi, Y.; Cheng, Y.; Zheng, Y.; Ruan, L. Q. Facile Immobilization of Heparin on Bioabsorbable Iron via Mussel Adhesive Protein (MAPs). *Prog. Nat. Sci. Mater. Int.* **2014**, *24* (5), 458–465.
- (76) Hernández, B.; Pflüger, F.; Derbel, N.; De Coninck, J.; Ghomi, M. Vibrational Analysis of Amino Acids and Short Peptides in Hydrated Media. VI. Amino Acids with Positively Charged Side Chains: L-Lysine and L-Arginine. *J. Phys. Chem. B* **2010**, *114* (2), 1077–1088.
- (77) Aliaga, A. E.; Garrido, C.; Leyton, P.; Diaz, F. G.; Gomez-Jeria, J. S.; Aguayo, T.; Clavijo, E.; Campos-Vallette, M. M.; Sanchez-Cortes, S. SERS and Theoretical Studies of Arginine. *Spectrochim. Acta. A. Mol. Biomol. Spectrosc.* **2010**, *76* (5), 458–463.
- (78) Sunatkari, A. L.; Talwatkar, S. S.; Tamgadge, Y. S.; Muley, G. G. Synthesis, Characterization and Optical Properties of L-Arginine Stabilized Gold Nanocolloids. *Nanosci. Nanotechnol.* **2015**, *5* (2), 30–35.
- (79) Ji, Z.; Santamaria, R.; Garzón, I. L. Vibrational Circular Dichroism and IR Absorption Spectra of Amino Acids: A Density Functional Study. *J. Phys. Chem. A* **2010**, *114* (10), 3591–3601.
- (80) Lopes, C. de C. A.; Limirio, P. H. J. O.; Novais, V. R.; Dechichi, P. Fourier Transform Infrared Spectroscopy (FTIR) Application Chemical Characterization of Enamel, Dentin and Bone. *Appl. Spectrosc. Rev.* **2018**, *53* (9), 747–769.
- (81) Fredi, G.; Simon, F.; Sychev, D.; Melnyk, I.; Janke, A.; Scheffler, C.; Zimmerer, C. Bioinspired Polydopamine Coating as an Adhesion Enhancer Between Paraffin Microcapsules and an Epoxy Matrix. *ACS Omega* **2020**, *5* (31), 19639–19653.
- (82) Ko, A. C.-T.; Choo-Smith, L.-P.; Hewko, M.; Leonardi, L.; Sowa, M. G.; Dong, C. C. S.; Williams, P.; Cleghorn, B. Ex Vivo Detection and Characterization of Early Dental Caries by Optical Coherence Tomography and Raman Spectroscopy. *J. Biomed. Opt.* **2005**, *10* (3), No. 031118.
- (83) Koutsopoulos, S.; Dalas, E. The Crystallization of Hydroxypatite in the Presence of Lysine. *J. Colloid Interface Sci.* **2000**, *231* (2), 207–212.